REST corepressors RCOR1 and RCOR2 and the repressor INSM1 regulate the proliferation–differentiation balance in the developing brain

Caitlin E. Monaghan[a], Tamilla Nechiporuk[a], Sophia Jeng[b], Shannon K. McWeeney[b], Jianxun Wang[c,d,e], Michael G. Rosenfeld[c,d], and Gail Mandel[a,1]

[a]Vollum Institute, Oregon Health and Science University, Portland, OR 97239; [b]Division of Bioinformatics and Computational Biology, Department of Medical Informatics and Clinical Epidemiology, Knight Cancer Institute, Oregon Health and Science University, Portland, OR 97239; [c]Howard Hughes Medical Institute, University of California, San Diego, La Jolla, CA 92093; [d]Department of Medicine, University of California, San Diego, La Jolla, CA 92093; and [e]School of Life Sciences, Beijing University of Chinese Medicine, No. 11 Bei San Huan Dong Lu, Beijing 100029, China

Contributed by Gail Mandel, December 12, 2016 (sent for review November 10, 2016; reviewed by Sadhan Majumder and Mark F. Mehler)

The transcriptional events that lead to the cessation of neural proliferation, and therefore enable the production of proper numbers of differentiated neurons and glia, are still largely uncharacterized. Here, we report that the transcription factor Insulinoma-associated 1 (INSM1) forms complexes with RE1 Silencing Transcription factor (REST) corepressors RCOR1 and RCOR2 in progenitors in embryonic mouse brain. Mice lacking both RCOR1 and RCOR2 in developing brain die perinatally and generate an abnormally high number of neural progenitors at the expense of differentiated neurons and oligodendrocyte precursor cells. In addition, *Rcor1/2* deletion detrimentally affects complex morphological processes such as closure of the interganglionic sulcus. We find that INSM1, a transcription factor that induces cell-cycle arrest, is coexpressed with RCOR1/2 in a subset of neural progenitors and forms complexes with RCOR1/2 in embryonic brain. Further, the *Insm1*$^{-/-}$ mouse phenocopies predominant brain phenotypes of the *Rcor1/2* knockout. A large number of genes are concordantly misregulated in both knockout genotypes, and a majority of the down-regulated genes are targets of REST. *Rest* transcripts are up-regulated in both knockouts, and reducing transcripts to control levels in the *Rcor1/2* knockout partially rescues the defect in interganglionic sulcus closure. Our findings indicate that an INSM1/RCOR1/2 complex controls the balance of proliferation and differentiation during brain development.

neurogenesis | RCOR1 | RCOR2 | INSM1 | REST

The development of the nervous system is an intricately orchestrated series of events beginning with formation of neuroepithelia. Progenitors that emerge from neuroepithelial stem cells undergo several proliferative transitions before ceasing to divide and terminally differentiating into neurons and glia. Both maintenance of the proliferative state and terminal transition to differentiated neurons and glia are regulated, in part, by chromatin-modifying proteins that are recruited to genes by specific transcription factors. In many cases, however, chromatin-modifying proteins have only been studied in vitro, and their roles in vivo remain unknown. For example, a protein whose importance in epigenetic regulation of neural genes has been recognized is RE1 Silencing Transcription factor (REST) Corepressor 1 (RCOR1) (1, reviewed in ref. 2). RCOR1 was identified originally as a direct binding partner for the master transcriptional regulator of neural genes, REST (3–5). The REST/RCOR1 complex has been studied primarily in cultured stem/progenitor cells, neurons, and glia (6–9). Like many other adaptor proteins in transcriptional complexes, RCOR1 does not have intrinsic enzymatic activity but rather binds directly to chromatin-modifying enzymes including histone deacetylases 1 and 2 (HDAC1/2) and the histone demethylase KDM1A (LSD1) (10–12). A related protein, RCOR2, shares ∼90% homology with RCOR1 in the ELM2 and SANT functional domains (13) and is also found in complexes with KDM1A and HDAC1/2 (14). Furthermore, RCOR2 is recruited by some of the same RCOR1-associated transcription factors, including REST, GFI1B, and ZMYND8 (15, 16). Despite knowledge of their cell-specific roles in some contexts (2, 17), the importance of RCOR1/2 in brain development has yet to be established definitively.

Here, we have generated knockout mice lacking both RCOR1 and RCOR2 in nestin+ neural progenitors (*Rcor1/2* KOs) to circumvent the potential for redundancy. The mice die perinatally and have smaller brains compared with controls. The neural progenitor domains are greatly expanded in the *Rcor1/2* KO embryonic brain, reflecting a larger number of progenitor cells, and numbers of mature neurons and oligodendrocyte precursor cells (OPCs) are reduced significantly compared with controls. We identify the repressor Insulinoma-associated 1 (INSM1) as a factor in complexes with RCOR1 and RCOR2 in embryonic brain. Elimination of INSM1 partially recapitulates the *Rcor1/2* KO phenotype. Transcript profiling analysis indicates that many of the same genes are misregulated in the *Rcor1/2* KO and the *Insm1*$^{-/-}$ mouse, including *Rest*, which is up-regulated, and REST targets that are down-regulated. Normalization of REST levels in the *Rcor1/2* KO through heterozygous loss of REST (18) partially rescues the morphological defects of the interganglionic sulcus (IGS). Our study identifies the INSM1–RCOR1/2 complex as an important contributor to the balancing of proliferation and differentiation during brain development.

Significance

Nervous system development involves a delicate balance between neural progenitor proliferation and neuronal differentiation. Repressors and corepressors each affect this balance, but in many cases, existence of the complexes in vivo has not been shown. Here, we identify a repressor/corepressor complex in embryonic brain consisting of Insulinoma-associated 1 (INSM1) and the RE1 Silencing Transcription factor (REST) corepressors RCOR1 and RCOR2. Elimination of RCOR1 and RCOR2, or INSM1, robustly promotes neural proliferation over neuronal and oligodendrocyte differentiation. Further, their elimination results in overexpression of REST, a direct target gene of INSM1. Normalizing REST levels in the RCOR1/2-deficient brain partially restores aberrant brain morphology. Our results identify a repressor complex required for critical events during normal brain development.

Author contributions: C.E.M., T.N., and G.M. designed research; C.E.M. performed research; J.W. and M.G.R. contributed new reagents/analytic tools; C.E.M., S.J., S.K.M., and G.M. analyzed data; and C.E.M. and G.M. wrote the paper.

Reviewers: S.M., University of Texas M.D. Anderson Cancer Center; and M.F.M., Albert Einstein College of Medicine.

The authors declare no conflict of interest.

[1]To whom correspondence should be addressed. Email: mandelg@ohsu.edu.

This article contains supporting information online at www.pnas.org/lookup/suppl/doi:10.1073/pnas.1620230114/-/DCSupplemental.

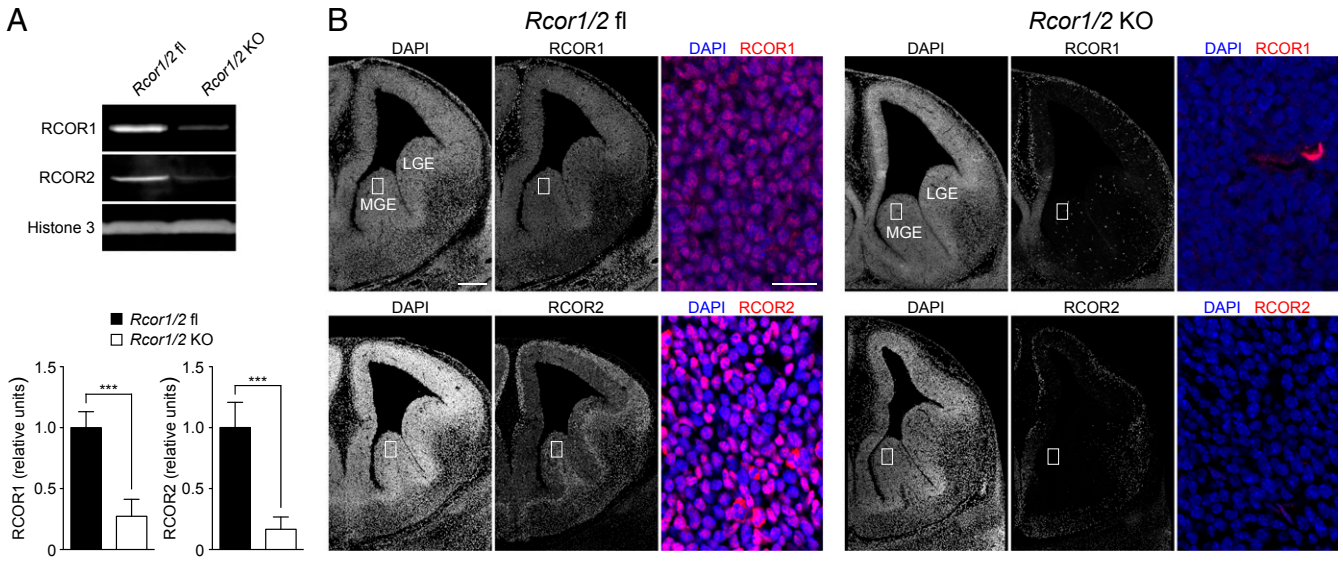

Fig. 1. Analysis of RCOR1 and RCOR2 expression at E13.5 in the *Rcor1/2* fl and *Rcor1/2* knockout mice. (*A*) Western blot analysis. RCOR1 and RCOR2 levels were normalized to histone H3 levels. The means and SDs are indicated. Statistical significance was assessed by *t* test ($n = 4$ mice). ***$P < 0.001$. (*B*) Representative immunohistochemistry on coronal hemisections of control (*Rcor1/2* fl) and *Rcor1/2* KO telencephalon labeled with the indicated antibodies and DAPI to mark nuclei. Boxes indicate regions shown at higher magnification to the right. (Scale bars, 200 μm and 20 μm.) LGE, lateral ganglionic eminence; MGE, medial ganglionic eminence.

Results

Deletion of Both *Rcor1* and *Rcor2* Genes Results in Embryonic Lethality and Severe Brain Phenotypes. We first generated individual brain-targeted KOs for RCOR1 and RCOR2 using nestin-Cre (Nes-Cre) (19) and floxed alleles of *Rcor1* or *Rcor2*. Generation of the *Rcor1*$^{fl/fl}$ mouse was described previously (20). We generated a mouse line containing floxed *Rcor2* alleles (*Rcor2*$^{fl/fl}$), in which Cre-mediated excision removes exons 5–9 (Fig. S1). This prevents expression of all but the first 88 amino acids, which contain part (the first 45 of 86 amino acids) of the ELM2 domain but neither SANT domain. Both KO mice lived to adulthood. Although some *Rcor1* KOs had small clefts in the ventricular zone (VZ) of the lateral subpallium that were not present in Nes-Cre controls, the other *Rcor1* KOs and all *Rcor2* KOs were indistinguishable from controls (Fig. S2). Hypothesizing that the RCOR proteins were to some extent compensating for each other, we generated an *Rcor1*$^{fl/fl}$; *Rcor2*$^{fl/fl}$; Nes-Cre mouse (*Rcor1/2* KO). PCR analysis of brain genomic DNA confirmed the expected excision events in the *Rcor1/2* KO.

Western blot analysis of nuclear extracts from E13.5 brain showed that RCOR1 and RCOR2 protein levels were reduced to 27.3 ± 13.9% and 16.6 ± 10.1% of control (*Rcor1*$^{fl/fl}$; *Rcor2*$^{fl/fl}$, hereafter *Rcor1/2* fl) levels, respectively (Fig. 1*A* and Fig. S3). The reduced protein levels were reflected at the level of immunohistochemistry at E13.5 (Fig. 1*B*). Importantly, the VZs and sub-VZs (VZ/SVZ) of the lateral subpallium (ganglionic eminences), the focus of this study, were almost entirely devoid of both RCOR1 and RCOR2. RCOR1 and RCOR2 were still present in some cells of the ventral hippocampus/dorsal septum, cortex, and subpallial mantle (Fig. 1*B*). However, by E18.5, very few cells in the *Rcor1/2* KO expressed either RCOR1 or RCOR2. RCOR1 expression was limited to cells in the ventral hippocampus/dorsal septum and endothelial cells, whereas RCOR2 expression was limited to cells in the ventral hippocampus/dorsal septum and the neocortex (Fig. S4). It is likely that the presence of RCOR1 and RCOR2 in some cells in the KO represents mosaicism of the Cre expression due to the cell-type specificity of the nestin promoter.

Although *Rcor1/2* KO mice all died by P1, they were present at Mendelian ratios at E18.5 (23% of live embryos), which indicates that they died between E18.5 and P1. At E18.5, Nes-Cre control body weights (1,022 ± 105 mg) were lower than those of both *Rcor1/2* fl (1,149 ± 59 mg) and *Rcor1/2* KO (1,130 ± 59 mg) mice ($P < 0.01$ and $P < 0.05$, respectively). Six to seventeen embryos were analyzed per genotype. There was no statistical difference in body weight between *Rcor1/2* KO embryos and *Rcor1/2* fl controls ($P > 0.05$). However, the *Rcor1/2* KO brain weights were reduced to 82–85% of those of both *Rcor1/2* fl and Nes-Cre controls (Fig. 2*A*; Nes-Cre, 68.4 ± 3.8 mg; *Rcor1/2* fl, 70.7 ± 4.7 mg; *Rcor1/2* KO, 57.8 ± 3.7 mg).

Morphologically, the E18.5 *Rcor1/2* KO brains differed from those of Nes-Cre and *Rcor1/2* fl controls in numerous ways (Fig. 2*B* and Fig. S5). Notably, the VZ/SVZs, especially in the subpallium, were disproportionately large. Further, the IGS, which is the cavity separating the lateral and medial ganglionic eminences (LGEs and MGEs, respectively) until these structures coalesce between E15.5 and E16.5, persisted in the *Rcor1/2* KO at E18.5. In

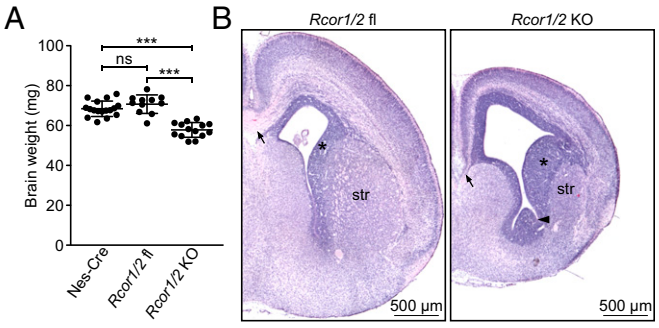

Fig. 2. Brain phenotypes of *Rcor1/2* knockouts at E18.5. (*A*) Brain weights of control (*Rcor1/2* fl and Nes-Cre) and *Rcor1/2* KO mice. The results represent, for each genotype, a minimum of 11 brains from five litters. Statistical significance was assessed using ANOVA followed by Tukey's multiple comparison test. ***$P < 0.001$; ns, not significant. (*B*) Representative H&E-stained coronal hemisections of *Rcor1/2* fl and *Rcor1/2* KO telencephalon. Note deep IGS (arrowhead), enlarged VZ/SVZs (*), and diminished corpus callosum (arrow) and axonal fasciculation in the striatum (str) in the KO compared with the control.

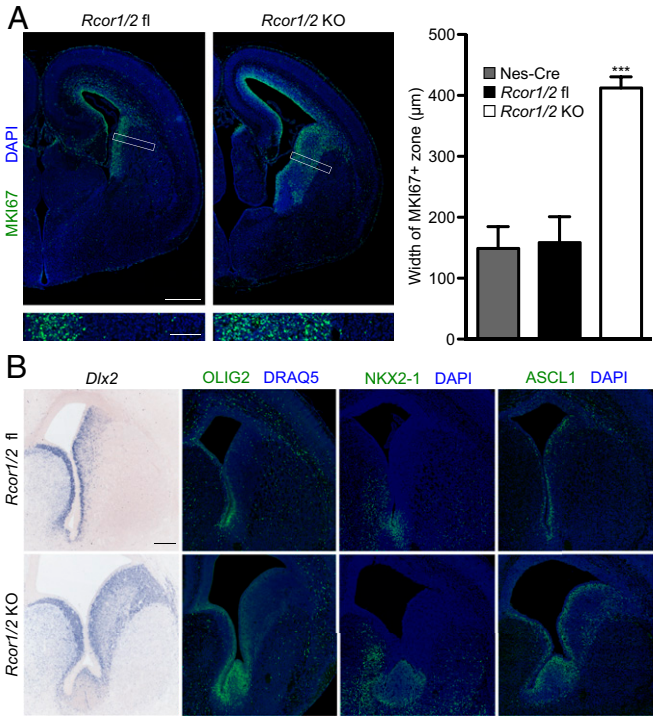

Fig. 3. Increased numbers of proliferating progenitors in E18.5 brains of *Rcor1/2* knockouts compared with controls. Sections labeled with antibodies were counterstained with DAPI or DRAQ5 to mark nuclei. (*A, Left*) Representative images of MKI67 immunohistochemistry. Boxes indicate *Insets* shown below at higher magnification. [Scale bars, 500 μm (*Top*) and 100 μm (*Bottom*).] (*Right*) Quantification of the width of the MKI67+ region in indicated controls and the *Rcor1/2* KO. Measurements were taken from images comparable to *Insets*. The means and SDs are indicated. Statistical significance was assessed by *t* test ($n = 5$ mice). ***$P < 0.001$. (*B*) Representative in situ hybridization histochemistry for *Dlx2* and immunohistochemistry for OLIG2, NKX2-1, and ASCL1. (Scale bar, 200 μm.)

addition, the neocortices in the KO brains were abnormally thin. Multiple axonal tracts were also affected: The corpus callosum never fully developed, axons traversing the striatum were either defasciculated or absent, and the anterior commissure was narrow (Fig. 2*B* and Fig. S5). In the hippocampus, the dentate gyrus and CA3 failed to develop into distinct structures. The thalamus and hypothalamus were hypoplastic (Fig. S5). Taken together, these abnormalities demonstrate that telencephalic development in the *Rcor1/2* KO was severely compromised.

***Rcor1/2* KOs Have More Neural Progenitors but Fewer Neurons and OPCs than *Rcor1/2* fl Controls.** We hypothesized that the dramatic expansion of the subpallial VZ/SVZ in the KO was due to excessive proliferation. To test this hypothesis, we labeled sections from E18.5 brain with an antibody directed against MKI67 (Ki67), a marker for proliferating cells. Because the MKI67+ cells were not distributed homogeneously in the KO, we first measured the width between the lateral ventricle and the basal edge of the MKI67+ region in the lateral subpallium. The width was ~2.7 times as large in the *Rcor1/2* KO as in the controls (Fig. 3*A*; Nes-Cre, 149 ± 36 μm; *Rcor1/2* fl, 159 ± 42 μm; *Rcor1/2* KO, 412 ± 18 μm). Further, the increase in width in the KO reflected higher numbers of both proliferating cells (*Rcor1/2* fl, 686 ± 273 MKI67+ cells; *Rcor1/2* KO, 1470 ± 141 MKI67+ cells; $P = 0.0023$) and nonproliferating cells (*Rcor1/2* fl, 280 ± 67 MKI67– cells; *Rcor1/2* KO, 1,212 ± 166 MKI67– cells; $P < 0.0001$).

Next, we used in situ hybridization histochemistry and immunohistochemistry to confirm that the expanded population of proliferating cells consisted of neural progenitors and to ascertain whether a specific subpopulation of subpallial neural progenitors was affected in the *Rcor1/2* KO. More cells in *Rcor1/2* KOs, compared with *Rcor1/2* fl controls, expressed *Dlx2* transcripts and OLIG2, ASCL1 (MASH1), and NKX2-1 proteins, markers for progenitors in the lateral subpallium (Fig. 3*B*). This finding suggests that the mechanism preventing cessation of cell division in *Rcor1/2* KOs is common to all subpallial progenitors.

Given the increased number of progenitors and the smaller brain size in the *Rcor1/2* KO mice, we expected *Rcor1/2* KOs to have fewer differentiated neural cells. We therefore immunolabeled coronal sections of E18.5 brain for the mature pan-neuronal marker MAP2 and compared the MAP2+ area to the total area in each hemisection (Fig. 4*A*). We found that neurons made up a smaller proportion of each hemisection in *Rcor1/2*

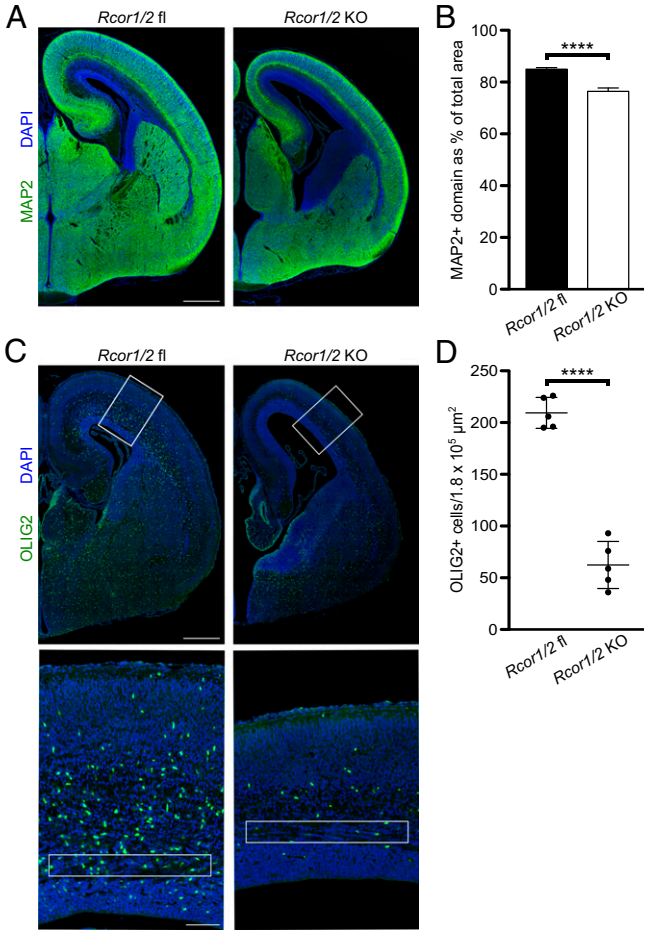

Fig. 4. *Rcor1/2* knockouts have fewer neurons and OPCs than controls. All analyses were performed on DAPI-labeled coronal sections from E18.5 brain. (*A*) Representative images of MAP2 immunohistochemistry. (Scale bar, 500 μm.) (*B*) Quantification of MAP2 immunolabeling, showing the percentage of each coronal hemisection occupied by the MAP2+ domain. The total area of the hemisection was determined on the basis of DAPI labeling. The means and SDs are indicated. Statistical significance was assessed with a *t* test ($n = 5$ mice). (*C*) Representative image of OLIG2 immunohistochemistry. Boxes in *Top* indicate regions shown below at higher magnification. Boxes in *Bottom* show the IZ of the neocortex. [Scale bar, 500 μm (*Top*) and 100 μm (*Bottom*).] (*D*) Quantification of OLIG2+ immunolabeling in the IZ of the neocortex. For each mouse, one region of 3×10^4 μm^2 was selected from each of six hemisections, and the numbers of OLIG2+ cells from all regions were added. Each mouse is represented by one dot. The means and SDs are indicated. Statistical significance was assessed by *t* test ($n = 5$ mice). ****$P < 0.0001$.

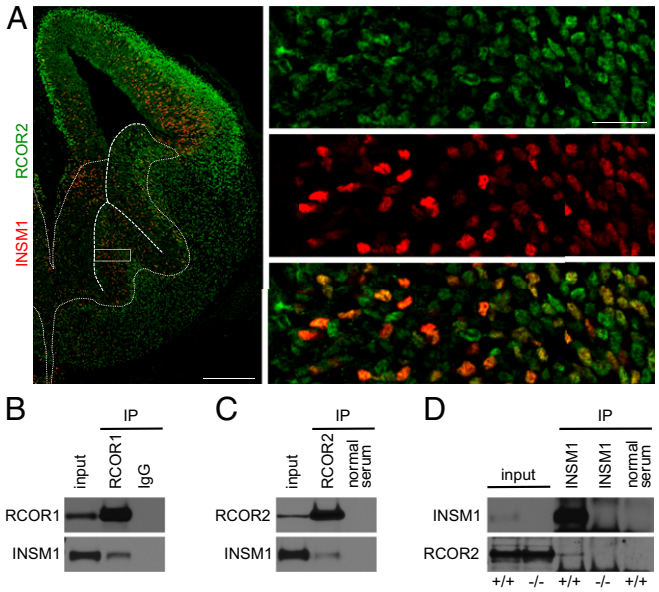

Fig. 5. RCOR1 and RCOR2 interact with INSM1 in subpallial neural progenitors. (*A*) Representative immunohistochemistry on a coronal hemisection of E13.5 telencephalon shows a subset of cells expressing both RCOR2 and INSM1. Dashed and dotted lines indicate the boundaries of the subpallial progenitor zone, determined by alignment of the section to an adjacent section immunolabeled with the subpallial progenitor marker ASCL1. Dashed lines indicate the borders between the subpallial progenitor zone and the lateral ventricle. Dotted lines indicate the boundaries between the subpallial progenitor zone and other brain regions. The box indicates the region shown to the right at higher magnification. [Scale bars, 200 μm (*Left*) and 20 μm (*Right*).] (*B–D*) Co-IP analysis for INSM1–RCOR1/2 complexes. IPs were performed on nuclear extracts prepared from E13.5 brain. Labels to the left of each blot indicate the antibodies used for Western blotting. IgG is rabbit IgG. Normal serum is rabbit serum in *C* and guinea pig serum in *D*. $^{+/+}$, *Insm1*$^{+/+}$ nuclear extracts; $^{-/-}$, *Insm1*$^{-/-}$ nuclear extracts.

KOs than in *Rcor1/2* fl controls (Fig. 4*B*; *Rcor1/2* fl, 84.9 ± 0.6% MAP2+; *Rcor1/2* KO, 76.5 ± 1.3% MAP2+).

To determine whether *Rcor1/2* KOs also had fewer OPCs, we performed OLIG2 immunolabeling. Embryonic OLIG2+ cortical cells are considered to be OPCs that have migrated from the ganglionic eminences (21). We determined the density of OLIG2+ cells in 3×10^4 μm^2 areas within the neocortical Intermediate Zone (IZ), which is the region between the cell-dense SVZ and the cortical subplate (Fig. 4*C*). *Rcor1/2* KOs had 70% fewer OLIG2+ cells per unit area than *Rcor1/2* fl controls (Fig. 4*D*; in 1.8×10^5 μm^2 of IZ representing the sum of six areas: *Rcor1/2* fl, 209 ± 15 cells; *Rcor1/2* KO, 62 ± 23 cells). To rule out the possibility that cell death was responsible for reduced numbers of differentiated neurons and OPCs in the *Rcor1/2* KOs compared with controls, we performed immunohistochemistry for activated caspase 3. We found very few positive cells in either *Rcor1/2* KO or *Rcor1/2* fl brain at E13.5 and E18.5.

RCOR1 and RCOR2 Are Coexpressed with the Transcription Factor INSM1 in Subpallial Neural Progenitors and Form Protein Complexes in Embryonic Brain. There are several transcription factors, such as REST, that recruit RCOR1 or RCOR2 to chromatin. But in the cases where these factors have been deleted from the developing brain in mice (18, 22, 23), the phenotypes did not resemble those of *Rcor1/2* KOs. One exception was the transcriptional repressor INSM1, which has been identified in complexes with RCOR1/2 in an endocrine cell line (24), is expressed in late neural progenitors (25), and has a germline knockout phenotype that resembles that of the *Rcor1/2* KO (26). However, no functional link has been established between RCOR1/RCOR2 and INSM1 in the developing nervous system.

To explore the possibility that an RCOR/INSM1 complex promotes neural differentiation, we first tested whether these proteins were coexpressed in neural progenitors. RCOR1 is expressed nearly ubiquitously and at uniform levels in neural progenitors (Fig. 1*B*). Although RCOR2 is also expressed ubiquitously within the brain at E13.5 (Fig. 1*B*), its expression level varies between cells in the neural progenitor domain: Periventricular progenitors, in particular, exhibited a wide range of RCOR2 expression levels, whereas abventricular progenitors consistently expressed high levels. INSM1 was not expressed in all progenitors but resembled RCOR2 in being expressed at a range of levels in periventricular progenitors and more uniformly in abventricular progenitors. Importantly, costaining for RCOR2 and INSM1 showed that many VZ/SVZ cells had moderate or high expression of both of these proteins (Fig. 5*A*).

Having established that all members of an RCOR1/RCOR2/INSM1 complex were expressed in a subset of VZ/SVZ cells, we performed coimmunoprecipitation (co-IP) analysis to test for complexes biochemically, using nuclear extracts from E13.5 brains. RCOR1 and RCOR2 immunocomplexes, but not immunoprecipitates of IgG or normal serum, each contained INSM1 (Fig. 5 *B* and *C* and Fig. S6). In a reciprocal experiment, RCOR2 was also present in INSM1 immunocomplexes from *Insm1*$^{+/+}$, but not *Insm1*$^{-/-}$, brain extracts. However, we were not able to interpret the parallel test for the presence of RCOR1 in INSM1 immunocomplexes due to nonspecific precipitation of RCOR1 from *Insm1*$^{-/-}$ brain by the INSM1 antibody (Fig. S6).

***Insm1*$^{-/-}$ Mice Phenocopy Aspects of the *Rcor1/2* KO Phenotype.** If INSM1 recruits RCOR1 and RCOR2 to facilitate neuronal and oligodendroglial differentiation, we would expect an *Insm1*$^{-/-}$ mouse (27) to exhibit a subset of phenotypes resembling those seen in the *Rcor1/2* KO mouse. Consistent with this idea, hematoxylin and eosin (H&E)-stained sections of E18.5 brain showed that the *Insm1*$^{-/-}$ mouse phenocopied two prominent features of the *Rcor1/2* KO phenotype (Fig. 6*A*). First, the *Insm1*$^{-/-}$ brain had an enlarged subpallial VZ/SVZ compared with its control, as had been noted previously (26). Second, *Insm1*$^{-/-}$ mice typically retained an IGS at E18.5 (Fig. 6*A*), although it was less pronounced and more variable than in *Rcor1/2* KO mice. In contrast, anatomical abnormalities of the corpus callosum, striatal axons, anterior commissure, hippocampus, thalamus, and hypothalamus in the *Rcor1/2* KO were not reproduced in *Insm1*$^{-/-}$ mice. This is not surprising, given that RCOR1 and RCOR2 are recruited by transcription factors other than INSM1.

To better assess the concordance between the *Rcor1/2* KO and *Insm1*$^{-/-}$ mice, we analyzed the expression of MKI67 in *Insm1*$^{-/-}$ mice. As in the *Rcor1/2* KO, we found that the distance between the lateral ventricle and the basal edge of the MKI67+ zone was more than twice as wide in *Insm1*$^{-/-}$ as in *Insm1*$^{+/+}$ mice (Fig. 6 *B* and *C*; *Insm1*$^{+/+}$, 103 ± 24 μm; *Insm1*$^{-/-}$, 256 ± 22 μm). And as in the *Rcor1/2* KO, this was due to increased numbers of both proliferating cells (*Insm1*$^{+/+}$, 531 ± 120 MKI67+ cells; *Insm1*$^{-/-}$, 789 ± 153 MKI67+ cells; $P = 0.0206$) and nonproliferating cells (*Insm1*$^{+/+}$, 312 ± 61 MKI67– cells; *Insm1*$^{-/-}$, 660 ± 122 MKI67– cells; $P = 0.0023$). Immunohistochemistry for ASCL1 confirmed that many cells in the expanded progenitor zone were indeed neural progenitors. The proportion of the brain expressing MAP2 (Fig. 6*D*) was significantly lower in *Insm1*$^{-/-}$ (83.2 ± 0.9%) than in *Insm1*$^{+/+}$ mice (86.7 ± 0.9%), although not as low as in the *Rcor1/2* KO. Similarly, there were fewer OLIG2+ cells in the IZ of the *Insm1*$^{-/-}$ mouse, but the reduction was more modest than that seen in the *Rcor1/2* KO (Fig. 6*E*; *Insm1*$^{+/+}$, 225 ± 27 cells; *Insm1*$^{-/-}$, 162 ± 15 cells; exploratory data analysis identified the sample indicated in red as an outlier, and it was removed from the analysis).

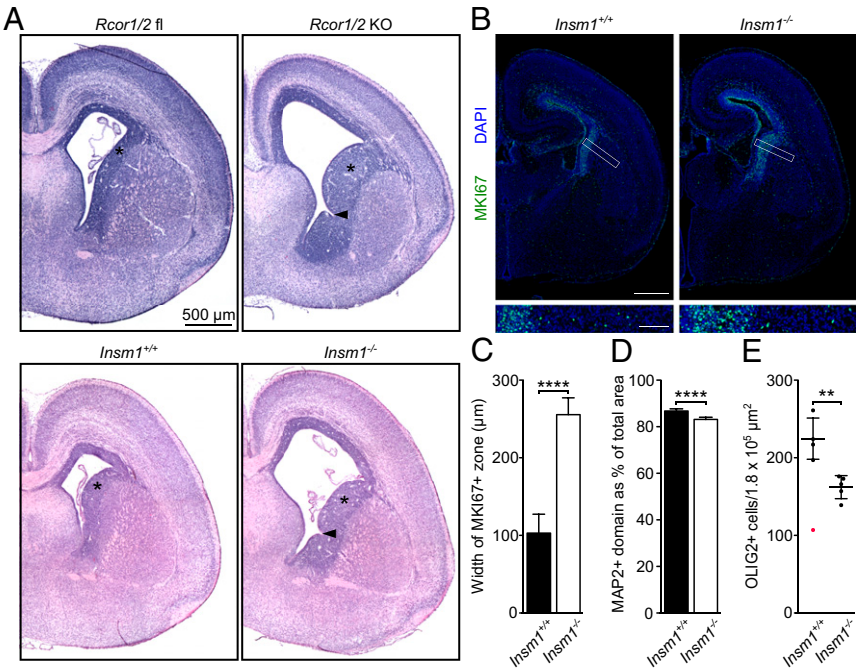

Fig. 6. *Insm1*$^{-/-}$ mice phenocopy several *Rcor1/2* knockout phenotypes in E18.5 brain. (*A*) H&E-stained E18.5 coronal hemisections. Asterisks indicate the VZ/SVZ; arrowheads indicate interganglionic sulci. (*B*) Representative hemisections immunolabeled for the proliferation marker MKI67 and counterstained with DAPI. Boxes indicate *Insets* shown below at higher magnification. [Scale bar, 500 μm (*Top*) and 100 μm (*Bottom*).] (*C*–*E*) Immunohistochemical analysis of coronal hemisections of *Insm1*$^{+/+}$ and *Insm1*$^{-/-}$ forebrain. Statistical significance was assessed by *t* tests. The means and SDs are indicated. (*C*) Quantification of the width of the MKI67+ zone. Measurements were made from areas comparable to those depicted in the *Insets* in *B*. (*D*) Quantification of MAP2 immunolabeling, showing the percentage of each E18.5 coronal hemisection occupied by the MAP2+ domain. (*E*) Quantification of the number of OLIG2+ cells in the IZ of the neocortex. For each mouse, one region of 3×10^4 μm^2 was selected from each of six hemisections, and the numbers of OLIG2+ cells from all regions were added. Each mouse is represented by one dot. Exploratory data analysis identified one wild-type count (107, indicated in red) as an outlier, so it was omitted from the statistical analysis. $^{**}P < 0.01$; $^{****}P < 0.0001$.

***Rcor1/2* KO and *Insm1*$^{-/-}$ Mice Share Many Common Misregulated Genes.** The above results suggested that INSM1 recruited RCOR1/RCOR2 to genes that must be repressed to promote neural differentiation. Therefore, we expected a shared subset of genes to be up-regulated in both the *Rcor1/2* and *Insm1* KOs. To test this expectation, we sequenced cDNA libraries made from the VZ/SVZ of the E13.5 MGE of each KO genotype as well as their respective controls (Dataset S1). We used ventral telencephalic progenitor cells because, in *Rcor1/2* KOs, this population showed the most complete loss of RCOR1 and RCOR2 at E13.5 as well as the most pronounced morphological abnormalities at E16.5 and thereafter. The VZ/SVZ, where neural progenitors were located, was isolated using laser capture microdissection (LCM).

For all analyses, we defined putative differential gene expression based on false discovery rate (FDR) adjusted P value < 0.05. Candidates that were also differentially expressed between the two controls (*Rcor1/2* fl and *Insm1*$^{+/+}$), as genes for which differential expression may have been independent of the loss of either INSM1 or RCOR1/2, were flagged and removed from downstream analyses. We examined both up- and down-regulated genes for each KO. Because RCOR1/2 and INSM1 are repressors, we expected many of the up-regulated genes to be direct targets of these proteins. In *Rcor1/2* KO and *Insm1*$^{-/-}$ mice, we identified 451 and 100 genes that were up-regulated, respectively. Twenty-one of the up-regulated genes were shared between the KOs (Fig. 7*A*, $P << 0.01$). This suggests that a common pathway is disrupted in both knockouts. We also identified 300 and 197 genes that were down-regulated, relative to the controls, in the *Rcor1/2* and *Insm1* KOs, respectively. These genes could be direct targets of RCOR1/RCOR2- or INSM1-mediated gene activation or could represent secondary effects of RCOR1/RCOR2- or INSM1-mediated repression. The overlap between the two genotypes was 105 genes (Fig. 7*A*, $P << 0.01$).

In contrast, very few genes (only six) were regulated oppositely in the two KOs, reinforcing our conclusion that the significance of the concordantly regulated genes was not spurious.

A Majority of the Genotype-Specific and Shared Down-Regulated Genes Are Targets of REST. Upon assessment of the candidate genes, it was noted that the majority of the down-regulated genes, 55% (166 of 300) in the *Rcor1/2* KO and 60% in the *Insm1*$^{-/-}$ mouse (118 of 197), had a functional REST binding site within two kilobases upstream of the transcription start site or within the DNA encoding the primary transcript (Dataset S2). Our identification of functional REST binding sites was based on a ChIP-seq analysis performed on mouse embryonic stem cells (ESCs) (28). We used ESC data because a previous study indicated that, in mice, all sites bound by REST in neural stem cells or fibroblasts were also bound by REST in ESCs, indicating that the ESC set is an inclusive set of REST targets (29). In contrast, REST binds a distinct set of targets in each neural subtype (6). Of the 105 down-regulated genes shared by the *Rcor1/2* and *Insm1* KOs, 64% (67) were REST targets (Fig. 7*B*). The proportion of REST targets is even higher among genes down-regulated by at least twofold [shared, 31 of 45 (69%); just *Rcor1/2* KO, 47 of 81 (58%); just *Insm1*$^{-/-}$, 21 of 35 (60%)]. In contrast, only a minority of up-regulated genes were REST targets [Fig. 7*B*; shared, 6 of 21 (29%); *Rcor1/2* KO alone, 148 of 430 (34%); *Insm1*$^{-/-}$ alone, 33 of 79 (42%)], which suggests that the large proportion of REST targets among the down-regulated genes is not simply a reflection of large numbers of differentially expressed REST targets.

The *Rest* Gene Is Up-Regulated in *Rcor1/2* and *Insm1* KOs. We sought to validate the mRNA profiling results using E13.5 MGE. To this end, we analyzed RNA from *Rcor1/2* and *Insm1* KOs by reverse transcription-quantitative PCR (RT-qPCR). We selected 8 (of 105) down-regulated genes that were shared between the genotypes based on the following criteria: Genes were down-regulated by at least twofold and detected at log cpm > 5 (cpm, counts per million). For seven of the eight genes, we observed statistically significant down-regulation in the *Rcor1/2* KO relative to the *Rcor1/2* fl control and the Nes-Cre control (Fig. 7*C*). In a separate experiment, we performed RT-qPCR to validate the *Insm1*$^{-/-}$ mRNA profiling results. Six of eight genes were significantly down-regulated compared with the *Insm1*$^{+/+}$ control, and one of the other two barely missed significance with a P value of 0.051 (Fig. 7*D*). Because a majority of the down-regulated genes contained REST binding sites (Fig. 7*B*), we asked whether REST expression was up-regulated in the KOs relative to controls. Although an increase in *Rest* expression was not detected from the mRNA profiling results, the RT-qPCR did show that REST expression was increased by more than twofold in the *Rcor1/2* KO (2.3-fold relative to Nes-Cre; 2.1-fold relative to

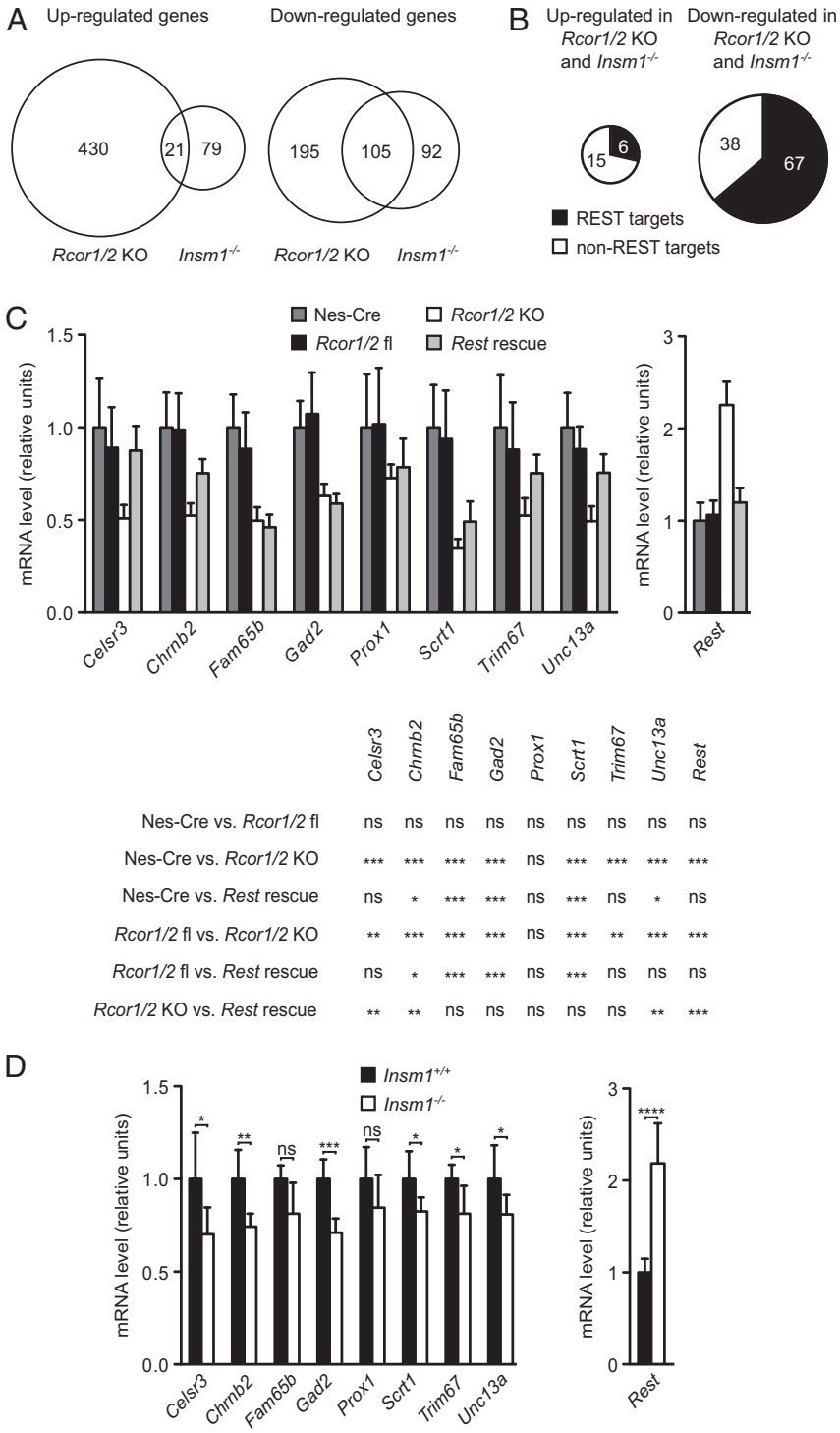

Fig. 7. Differential gene expression in *Rcor1/2* knockout and *Insm1*$^{-/-}$ mice at E13.5. (*A*) Venn diagrams comparing the genes misregulated in *Rcor1/2* KO and *Insm1*$^{-/-}$ mice (relative to *Rcor1/2* fl and *Insm1*$^{+/+}$ mice, respectively). (*B*) Proportions of up- and down-regulated genes that are REST targets. (*C*, *Top*) RT-qPCR analysis of cDNA prepared from E13.5 MGE. Each transcript quantity was normalized to the geometric mean of the quantities of four reference genes: *Aip*, *Cxxc1*, *Rn45s*, and *Rps20*. The means and SDs are indicated ($n = 6$ mice). (*Bottom*) Significance was determined by ANOVA with Tukey's multiple comparison tests on log-transformed data. (*D*) RT-qPCR analysis as described in *C*. Statistical significance was assessed using *t* tests with Welch's correction on log-transformed data. ns, $P > 0.05$; *$P < 0.05$; **$P < 0.01$; ***$P < 0.001$; ****$P < 0.0001$.

Rcor1/2 fl) and in the *Insm1*$^{-/-}$ mouse (2.2-fold relative to *Insm1*$^{+/+}$) (Fig. 7 *C* and *D*). We therefore hypothesized that the down-regulation of REST target genes in the two knockout mice was due to increased REST-mediated gene repression rather than to loss of INSM1/RCOR-mediated gene activation.

Normalizing *Rest* Expression in the *Rcor1/2* KO Increases Transcript Levels of Repressed REST Targets. To test whether normalizing *Rest* levels would rescue the major phenotypes in the *Rcor1/2* KO brains, we used mice with a *Rest* allele containing a conditional gene trap cassette. Cre-mediated recombination of this allele

results in the loss of mature *Rest* transcripts (18). We generated an *Rcor1*$^{fl/fl}$; *Rcor2*$^{fl/fl}$; *Rest*$^{GTi/+}$; Nes-Cre mouse (hereafter, *Rest* rescue), in which *Rest* transcript levels are equivalent to control levels (Fig. 7*C*). By RT-qPCR analysis, we found that of seven REST target transcripts down-regulated in the *Rcor1/2* KO, one of them, *Celsr3*, was restored fully to control levels in the *Rest* rescue (Fig. 7*C*). Three other transcripts were restored partially (*Chrnb2*, *Trim67*, and *Unc13a*), and three were not rescued (*Fam65b*, *Gad2*, and *Scrt1*).

Reduction of *Rest* Transcript to Control Levels in the *Rcor1/2* KO Ameliorates the IGS Phenotype. H&E staining showed that E18.5 *Rest* rescue mice exhibited less pronounced IGS than *Rcor1/2* KOs, as assessed by an investigator blinded to genotype. The difference between the KO and rescue phenotypes was most apparent at levels caudal to the peak depth of the IGS. In such sections, the IGS of the *Rcor1/2* KO is still quite large, whereas that of the *Rest* rescue is subtle or nonexistent (Fig. 8 and Fig. S7). However, in all other regards, the *Rest* rescues could not be distinguished visually from the *Rcor1/2* KOs. We therefore did not analyze MKI67 and MAP2 to evaluate the progenitor cell overabundance and neuronal differentiation phenotypes. Quantification of the number of OLIG2+ cells in the IZ of the neocortex indicated that this population was not rescued (in 1.8×10^5 μm^2 of IZ representing the sum of six areas: *Rest* rescue, 60 ± 12 cells; compare with Fig. 4*D*).

Discussion

In this study, we demonstrate the importance of RCOR1/2 corepressor function in mouse brain development. There was no prior in situ or immunohistochemical characterization of RCOR1 expression in early mouse brain development. An early in situ hybridization study mistakenly identified *Rcor3* as *Rcor1*, because it was performed before the mouse genome was completely annotated (30). Our analysis of control mice here indicates that RCOR1 is expressed nearly ubiquitously in the telencephalon at E13.5 and E18.5. We show that RCOR2 is also expressed nearly ubiquitously in E13.5 telencephalon but at higher levels in the abventricular progenitor zone and mantle layer than in the progenitors directly adjacent to the lateral ventricle. By E18.5, RCOR2 is no longer expressed ubiquitously, consistent with previous studies that suggested that *Rcor2* mRNA and protein levels diminish during late embryonic stages (31, 32). The overlapping expression of RCOR1 and RCOR2 in E13.5 telencephalon explains why they may compensate for each other in the single KOs. Indeed, *Rcor1* and *Rcor2* individual KOs were nearly normal (Fig. S2), in contrast to *Rcor1/2* KOs, which had profound brain phenotypes (Fig. 2). Future studies will determine whether, in a wild-type context, RCOR1/2 are found in the same or separate complexes and whether the two RCOR proteins have shared and/or distinct gene targets.

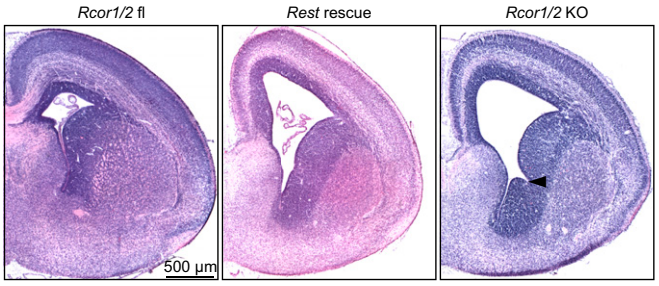

Fig. 8. Reducing *Rest* transcript levels to control levels in the *Rcor1/2* knockout partly rescues the IGS phenotype (arrowhead). Shown are representative H&E-stained coronal hemisections of telencephalon at E18.5.

While our studies were in progress, another group published that brain deletion of just *Rcor2* resulted in abnormal cortical development (32). However, the abnormalities were even more severe than those in our *Rcor1/2* KO, perhaps reflecting different genetic backgrounds of the KOs or a different Nes-Cre transgene.

Retention of the IGS at E18.5, progenitor overabundance, and reduced numbers of mature neurons and OPCs were major phenotypes in the *Rcor1/2* KO mouse. The role for chromatin-modifying complexes in these processes is poorly understood, particularly in regards to the transcription factors that recruit them. A strong candidate for recruiting RCOR1/2 to the chromatin is the repressor INSM1 (33). It causes cell-cycle arrest (34, 35) and is required for terminal differentiation of a variety of cell types (27, 36–40). Further, previous *Insm1* KO studies indicated that, similar to the *Rcor1/2* KO, the *Insm1* KO had a thin cortex and a thick PCNA+ proliferative region in E16.5 ventral telencephalon (26). However, the previous studies did not indicate whether the *Insm1* KO retained the IGS at E18.5 or had fewer OLIG2+ cells, two striking phenotypes in the *Rcor1/2* KO.

Because of the above findings, we performed co-IP analysis in embryonic brain and identified complexes containing both INSM1 and RCOR1 or RCOR2 proteins. This finding is consistent with a previous study identifying RCOR1/2 in complexes with INSM1 in an endocrine cell line (24). Another study detected *Insm1* transcripts in abventricular neural progenitors and nascent neurons (25). Our immunohistochemistry was consistent with this pattern, and we found the highest levels of INSM1 staining in cells surrounding the border between the SVZ and the mantle area, where both RCOR1 and RCOR2 are also highly expressed.

We compared the phenotypes in the *Insm1*$^{-/-}$ mouse (27) to those in the *Rcor1/2* KO. The *Insm1*$^{-/-}$ mouse exhibited an overabundance of progenitors, incomplete IGS closure, and deficient neurogenesis and oligodendrogenesis, although a few phenotypes observed in the *Rcor1/2* KO were not reproduced at all. Several studies indicate that RCOR1/2 are recruited by transcription factors other than INSM1, including factors expressed in the nervous system (5, 15, 41, 42). Further, RCOR1 binds to distinct sets of genomic targets in different neural cell types (6, 7, 9). These factors likely explain the discordance in some phenotypes between the KOs.

Two independent factors contribute to the reduction in neurons and OPCs in the *Rcor1/2* KO and *Insm1*$^{-/-}$ mouse. First, some neural progenitors fail to stop proliferating, as is demonstrated by the abnormally high numbers of MKI67+ cells in the subpallial progenitor zone of the knockouts compared with controls, and this keeps these cells from differentiating. Because increased numbers of progenitors were observed at multiple rostrocaudal levels in both knockouts and each of four different progenitor markers was expressed in more cells in *Rcor1/2* KOs than in controls (Fig. 3*B*), it seems likely that the propensity to continue dividing is a general problem affecting multiple subpopulations of subpallial progenitors. Second, specification and/or migration of neurons and/or OPCs is also perturbed, as is evidenced by the increased numbers of MKI67-negative cells in the progenitor zone of each knockout relative to its respective control. Because specification and migration are linked, it is generally difficult to distinguish between them, and we did not pursue experiments to address this difficult issue. However, supporting the possibility that neuronal migration might be inhibited, several genes required for neuronal migration, including *Celsr3* (cadherin EGF LAG seven-pass G-type receptor 3) (43), *Dcx* (doublecortin) (44), and *Dclk2* (doublecortin like kinase 2) (45), were down-regulated in both knockouts.

Given that INSM1 can potentially regulate many different target genes, is it possible to identify a molecular basis for the phenotypes that are shared in the *Rcor1/2* KO and *Insm1*$^{-/-}$ mice? Because INSM1 and RCOR1/2 repress transcription (1, 14, 33),

we anticipated that we would identify a set of shared up-regulated genes in the KOs. Although we did identify such genes, we were surprised to find even more shared down-regulated genes. Interestingly, 64% of the genes down-regulated in both the *Rcor1/2* and *Insm1* KOs were direct REST target genes. INSM1 binds to the REST promoter in vivo (27), suggesting that loss of INSM1 could cause derepression of *Rest*. Further, INSM1 is up-regulated at the transition from apical to basal progenitor (26), which corresponds precisely to the timing of REST down-regulation during embryogenesis (18). Together, these findings suggest that the INSM1–RCOR1/2 complex directly represses *Rest* and thus derepresses REST targets. We used RT-qPCR to confirm that *Rest* transcript levels were indeed elevated in the *Rcor1/2* KO and $Insm1^{-/-}$ mice compared with controls.

Another question that arises is whether increased REST protein could repress target genes in the absence of RCOR1 and RCOR2. Several studies have shown that REST can mediate repression independent of RCOR proteins by recruiting the corepressors SIN3A, SIN3B, or CDYL (46–49). For this reason, we hypothesized that overexpression of REST was causing repression of REST targets in the *Rcor1/2* KO. To test this hypothesis, we normalized REST levels in the *Rcor1/2* KO through heterozygous loss of *Rest*. This restored or partially restored transcript levels of some selected REST target genes, which demonstrated that REST was one of the factors contributing to their repression in the *Rcor1/2* KO and likely also in the $Insm1^{-/-}$ mouse. Normalizing REST levels partially repaired closure of the IGS. This suggests that the retention of the IGS in the *Rcor1/2* KO was due to repression mediated by the REST/SIN3 or REST/CDYL complexes. Unfortunately, we are not aware of any published work regarding mechanisms underlying the closure of the IGS. However, REST overexpression prevents neuronal migration in vivo by repressing *Dcx* (50), and as indicated above, several REST targets implicated in neuronal migration, including *Dcx*, were repressed in *Rcor1/2* and *Insm1* KOs. Thus, it is possible that REST overexpression prevents closure of the IGS by perturbing neuronal migration. Such a perturbation could occur if the neural progenitors responsible for remodeling the ventricular surface require instructive cues from migrating neurons. Future studies that manipulate REST target genes with potential functions in migration could shed new light on IGS closure.

The reason some abnormalities persisted in the *Rest* rescue is presumably that other targets of the INSM1/RCOR complex were responsible for these phenotypes. Likely targets include *Tgif1* and *Hey1*, which were up-regulated in both the *Rcor1/2* KO and the $Insm1^{-/-}$ mice. These genes encode transcriptional repressors involved in neural development (51, 52) and are expressed widely in neural progenitors but down-regulated in neurons (52, 53).

Both *Insm1* and *Rcor1/2* have homologs in *Caenorhabditis elegans* (54, 55). Interestingly, *C. elegans* that are mutant for the *Insm1* homolog *egl-46* have a phenotype similar to what we observe in the $Insm1^{-/-}$ and *Rcor1/2* KO mice. In these worms, certain neural progenitors also undergo aberrant additional rounds of cell division (54, 56). In the mammalian subpallium, which produces a greater variety of neural cell types than the worm nervous system, INSM1 and RCOR1/2 regulate the production of OPCs as well as of neurons. Altogether, our studies suggest that an INSM1/RCOR complex facilitates neuronal and oligodendroglial differentiation.

Materials and Methods

Mice. All animal studies were approved by the Oregon Health and Science University Institutional Animal Care and Use Committee. $Rcor1^{fl/fl}$, Nes-Cre, and $Rest^{GTi/GTi}$ mice have been described previously (18–20). $Rcor2^{fl/fl}$ mice were generated by targeted mutagenesis in ESCs. Two *loxP* sites were inserted flanking exons 5–9 of *Rcor2* (Fig. S1; exons are numbered relative to uc008gkn.2). Correct targeting was confirmed by Southern blotting with 5′ and 3′ external probes. The $Rcor2^{fl/fl}$ mice are available at the Jackson Laboratory as stock no. 030004. The above mice were backcrossed into a C57BL/6J background for at least 10 generations. $Insm1^{+/-}$ (27) mice were acquired on a mixed background from the Mutant Mouse Resource and Research Centers (036986-JAX). Founders were crossed to CD-1 mice for one generation (36), and the offspring were interbred for one to four generations to produce the embryos used in experiments. In this mixed background, ∼50% of the $Insm1^{-/-}$ embryos survived to E18.5. Pregnancies were timed on the basis of observation of a coital plug, with the morning that the plug was observed defined as E0.5. The following primers were used for genotyping: Cre [646 base pairs (bp)], GCTAAACATGCTTCATCGTCGG and GATCTCCGGTATTGAAACTCCAGC; $Rcor1^{fl}$ (481 bp) versus $Rcor1^{+}$ (390 bp) (20), GTAGTTGTCTTCAGACACTCCAGA and GGGAAGCTCATCTATAGGCAA; $Rcor1^{fl}$ (1,199 bp) or $Rcor1^{+}$ (1,006 bp) versus $Rcor1^{rec}$ (336 bp) (20), ATTTGTGTCATGTGTCATGTA and GGGAAGCTCATCTATAGGCAA; $Rcor2^{fl}$ (315 bp) versus $Rcor2^{+}$ (143 bp), TCCGAGGTCTTGACTCACAGC and CAGGCTTGACACTGCACCATT; $Rcor2^{rec}$ (365 bp), AATTCTGCTCATCCTTTCAGA and CAGGCTTGACACTGCACCATT; $Insm1^{-/-}$ (∼550 bp) versus $Insm1^{+/+}$ (447 bp) (protocol from Jackson Labs), CCTTGTACAACCGACAGCTCT and GTGCCCTGTATCTGCTGTGC; $Rest^{+}$ (478 bp) (18), TGGATGTTGAGGTCCGTTGTG and GGCTACGGATCCCTTCTTCCC; $Rest^{GTi}$ (782 bp) (18), CTCCGCCTCCTCTTCCTCCAT and TTTGAGGGGACGACGACAGTA; $Rest^{GTreinv}$ (518 bp) (18), CTCCGCCTCCTCTTCCTCCAT and CCTCCCCCGTGCCTTCCTTGA.

Antibodies. Primary antibodies used for immunohistochemistry are listed in Table S1. The following Alexa Fluors from Thermo Fisher Scientific were used for immunohistochemistry (1:2,000): 555 goat anti-mouse IgG (A21424), 568 donkey anti-rabbit IgG (A10042), 555 goat anti-mouse IgG (A21424), 555 goat anti-rabbit IgG (A21429), 568 goat anti-rabbit IgG (A11011), 488 goat anti-rabbit IgG (A11034), 647 goat anti-guinea pig IgG (A21450), and 555 goat anti-mouse IgG2a (A21137). CF647 goat anti-mouse IgG (20281) and IgG1 (20252) from Biotium were also used for immunohistochemistry (1:2,000). For the Western blot in Fig. 1, we used mouse anti-RCOR1 (NeuroMab clone K72/8, diluted 1:1,000), rabbit anti-RCOR2 (in house-generated rabbit serum recognizing the N terminus of human RCOR2; 1:10,000), rabbit anti-histone H3 (Cell Signaling 9715; 1:1,000), anti-rabbit IR680 (ThermoPierce 35569; 1:5,000), and anti-mouse IR800 (Rockland 610–132-121; 1:5,000). For IPs, the following antibodies were used: rabbit polyclonal antibody for RCOR1 (47), rabbit IgG (Jackson ImmunoResearch 011–000-002), rabbit anti-RCOR2 (described above), normal rabbit serum (Jackson ImmunoResearch 011–000-120), guinea pig INSM1 antiserum (which was a generous gift from Carmen Birchmeier, Max Delbrück Center for Molecular Medicine, Berlin), and normal guinea pig serum (Jackson ImmunoResearch 006–000-001). For Western blotting following IPs, the same RCOR1, RCOR2, and INSM1 antibodies were used at concentrations of 1:1,000, 1:10,000, and 1:10,000, respectively. We also used horseradish peroxidase-conjugated mouse anti-rabbit IgG (light chain only; Jackson ImmunoResearch 211–032-171; 1:4,000) and horseradish peroxidase-conjugated donkey anti-guinea pig IgG (heavy and light chains, Jackson ImmunoResearch 706–035-148, 1:10,000).

Western Blotting. Nuclei were prepared from E13.5 brain extracts as described (57), resuspended in RIPA buffer, treated with Benzonase, homogenized with a motorized pestle, and centrifuged to remove particulates. Protein concentrations of supernatants were quantified using a Pierce BCA Protein Assay Kit. Twenty-microgram samples were separated on a NuPAGE Novex 4–12% (wt/vol) Bis–Tris gel and transferred to a nitrocellulose membrane (GE Healthcare 10600001) at 100 V at 4 °C for 2 h. The membrane was exposed to primary antibodies overnight at 4 °C and to secondary antibodies for 1 h at room temperature. The membrane was imaged with a LI-COR Odyssey CLx using AutoScan. Background-subtracted signal intensity was quantified using Image Studio 4.0 software. For each sample, the levels of RCOR1 and RCOR2 signal were normalized to the level of histone H3.

Immunohistochemistry. Embryos were transcardially perfused with 4% (vol/vol) formaldehyde in PBS. For E18.5 embryos, the brain was dissected, and in some cases postfixed at 4 °C overnight, before being frozen and cryosectioned. For E13.5 embryos, the head was frozen intact. Sections were prepared for blocking in one of three ways, depending upon the antibody (indicated in Table S1). Blocking and antibody labeling were performed with either a mouse-on-mouse kit (Vector Labs BMK-2202) or 5% (vol/vol) normal serum and 0.125% BSA in PBS-Triton. All slides were blocked for 1 h at room temperature and labeled with primary antibody at 4° overnight and then at 37 °C for 2 h (with the exception of MAP2 and TUBB3 antibodies, with which the 37° step was omitted). Slides were then rinsed three times with PBS-Triton, treated with secondary antibodies and a DNA dye [either DAPI (4′,6-diamidino-2-phenylindole) or DRAQ5 (Deep Red Anthraquinone 5)] at room temperature for 1–2 h, rinsed four times with PBS-Triton, rinsed once with

PBS, and coverslipped after application of Prolong Gold Antifade Mountant (Thermo Fisher Scientific P36930).

H&E Staining. Twenty-micrometer sections were prepared from E18.5 brains as described above, with the overnight 4° postfixation step included. The sections were fixed with 4% (vol/vol) formaldehyde in PBS for 15 min and then stained with H&E.

Image Analysis. Immunofluorescent images were acquired using a Zeiss LSM 710 confocal microscope. Images intended to be compared with one another were acquired under the same conditions and processed identically. For quantifications, matching sections from each of five animals per genotype were used. Images were processed using ImageJ and Photoshop CS4 and were analyzed by an experimenter blinded to genotype.

In Situ Hybridization. *Dlx2* probes (58) containing digoxigenin-11-UTP were treated with DNase I to remove the template and purified with either a QIAGEN RNeasy Mini Kit or a PureLink RNA Mini Kit. Probes were diluted to 1 μg/mL with prehybridization solution [50% (vol/vol) formamide; 5× SSC, pH 4.5; 50 μg/mL yeast tRNA; 1% SDS; 50 μg/mL heparin]. Brain sections were prepared in the same way as for H&E staining. Slides were hybridized with probe as previously described (59). After hybridization, slides were washed three times each with wash solution 1 [50% (vol/vol) formamide; 4× SSC, pH 4.5; 1% SDS] at 70 °C, wash solution 2 [50% (vol/vol) formamide; 2× SSC, pH 4.5] at 65 °C, and TBST (50 mM Tris, 150 mM NaCl, 0.1% Tween-20) at room temperature. Sections were blocked with 5% (vol/vol) normal sheep serum in TBST and incubated overnight at 4° with antidigoxigenin Fab fragments conjugated to alkaline phosphatase (Roche 11093274910) diluted 1:2,000. Sections were washed four times with TBST and three times with coloration buffer (100 mM Tris·HCl, pH 9.5; 100 mM NaCl; 0.1% Tween-20) and developed using NBT/BCIP Stock Solution (Roche 11681451001). Sections were fixed with 4% (wt/vol) PFA and 0.1% glutaraldehyde in PBS; progressively dehydrated with 50%, 75%, 95%, and 100% (vol/vol) ethanol; infiltrated with xylenes; dabbed with Permount (Fisher Scientific SP15); and coverslipped. In situ hybridization was performed on sections representing three distinct rostral-caudal positions for each of three *Rcor1/2* fl controls and three *Rcor1/2* KOs.

Co-IP. Nuclear pellets were prepared as described (57) but with inclusion of phosphatase inhibitors (Millipore 524628) and 1 mM phenylmethylsulfonyl fluoride in the tissue cracking and nuclear buffers. After being washed with nuclear buffer, each pellet was resuspended in lysis buffer [50 mM Tris, pH 7.4; 140 mM NaCl; 1% Triton X-100; 2 mM $MgCl_2$; protease inhibitors without EDTA (Roche); phosphatase inhibitors (Millipore 524628); 1 mM sodium orthovanadate] (24). Samples were homogenized with a motorized pestle. IPs were performed as described (24) using 10 μg of antibody and 65 μL of Protein A Dynabeads (Invitrogen 10002D) for every 1.5 mg protein lysate (~20 brains). Proteins were eluted from the beads with glycine, residual proteins were eluted by boiling in NuPAGE LDS Sample Buffer (Invitrogen NP0007) containing 300 mM DTT, and the eluates were combined. Samples were run on a 3–8% (wt/vol) NuPAGE Novex Tris-Acetate Gel (Invitrogen EA03785BOX). Each input lane was loaded with 15 μg of protein, and each IP lane was loaded with the volume of immunoprecipitate corresponding to 200 μg of input. After transfer, nitrocellulose membranes were incubated with primary antibodies overnight at 4 °C and with secondary antibodies conjugated to horseradish peroxidase for 1 h at room temperature. Membranes were treated with SuperSignal West Pico Chemiluminescent Substrate (Thermo Scientific 34080) and exposed to X-ray film. Each IP was performed at least twice.

RNA Profiling. Brains were dissected from E13.5 embryos, embedded in Tissue Freezing Medium, frozen, cut into 10-μm coronal sections at –25°, and loaded onto poly-L-lysine–coated PEN-membrane slides (Zeiss 415190–9041-000). Immediately after sectioning, slides were stained with an abbreviated hematoxylin staining protocol. A cell-dense region roughly equivalent to the VZ/SVZ of the MGE was isolated using LCM with a Zeiss PALM MicroBeam. Tissue was pooled to make two samples of three embryos for each of four genotypes: *Rcor1/2* fl, *Rcor1/2* KO, *Insm1*$^{+/+}$, and *Insm1*$^{-/-}$. RNA was extracted using a QIAGEN RNeasy Micro Kit in accordance with the instructions, except that each sample was incubated in Buffer RLT containing 0.1% β-mercaptoethanol for 30 min at room temperature before starting. cDNA Libraries were made by the OHSU Massively Parallel Sequencing Shared Resource. A BioAnalyzer 2100 confirmed that all samples had RNA integrity numbers ≥ 9.3. Each cDNA library was made from either 300 ng (*Rcor1/2* fl and *Rcor1/2* KO) or 500 ng (*Insm1*$^{+/+}$ and *Insm1*$^{-/-}$) of RNA using the Illumina TruSeq RNA Prep Kit v2. Library quality was assessed using a TapeStation 2200, and libraries were quantified by qPCR using a KAPA Library Quantification Kit. Libraries were sequenced using 100-cycle single-read runs on a HiSeq 2500.

Sample quality was assessed using Fastqc (v0.11.3). To address technical artifacts, we trimmed 3 bp from the 5′ end and 1 bp from the 3′ end. We aligned each sample to the mm10 genome using Subread (60) and aggregated transcript counts using featureCounts (61). Transcript counts were aggregated at the gene level to perform gene-level differential expression analysis. Differential expression analysis was conducted using edgeR (62). Data were normalized using TMM (Trimmed Mean of M-Values). *P* values were adjusted for multiple comparisons using the Benjamini–Hochberg correction (63). Putative differential expression was based on FDR-adjusted *P* value < 0.05.

To test whether the number of concordantly up-regulated genes was significant, we performed a simulation of the amount of overlap achieved if 451 (number of genes up-regulated in the *Rcor1/2* KO) and 100 (number of genes up-regulated in the *Insm1*$^{-/-}$ mouse) genes were sampled randomly and independently from the total pool of 30,737 genes. We performed the sampling 10^6 times to determine the distribution of possible overlaps. We performed a comparable simulation, sampling 300 and 197 genes, to determine whether the number of concordantly down-regulated genes was significant. The 99th percentile of the random sampling was five for the up-regulated genes and six for the down-regulated genes, compared with the observed values of 21 and 105, respectively. To be conservative, we report this as $P << 0.01$ (calculations with hypergeometric distribution were $P < 1.389 \times 10^{-18}$ and $P < 3.639 \times 10^{-163}$, respectively).

RT-qPCR. RT-qPCR was performed on manually microdissected MGEs. Tissue was homogenized in 1 mL TRIzol (Thermo Fisher 15596026) with a motorized pestle. RNA extraction was performed with the PureLink RNA Mini Kit (Thermo Fisher 12183025), including on-column DNase treatment (Thermo Fisher 12185010). After extraction, RNA was precipitated with sodium acetate and ethanol, resuspended in water, and quantified with a NanoDrop 2000. Samples of 600 ng RNA were reverse-transcribed with the SuperScript III First Strand Synthesis System (Thermo Fisher 18080–051) using random hexamers. RT-qPCR was performed on a QuantStudio 6 Flex Real-Time PCR System using Power SYBR Green PCR Master Mix (Applied Biosystems #4367659) and 300 nM of each primer (with the exception of the *Prox1* primers, which were used at 900 nM each). The following primers were used: *Celsr3*, TGCTGTGAGGACAGCTCCTA and CTTCAGGACCAGTCGGAAAC; *Chrnb2*, GATGATGACCAGAGTGTGAGG and GGTCCCAAAGACACAGACAA; *Fam65b*, CCGCAGCTACAAGGAATACA and CCAGCCAGACCTTTCATCTT; *Gad2*, CTGTGCGCTCTGCTCTATG and AGAAACGCGTAGTTGACATCC; *Prox1*, AAAGAACAGAAGCGAGAGGAG and GCTGTCATAGACCTGGTAGAAC; *Scrt1*, GGTCAAACTTGACACATTCTCTTC and CGTAGTCACTGAGGTATCCTTTATC; *Trim67*, CCCATACCAACAGGACTGAAG and CTGTTGCCCATTGATGAAGAAG; *Unc13a*, GAAGGTGCAGAACGTGAAGA and GCGGTTGATCTCAAACATGAAG; *Rest*, GGCTGCTCTCAAGGAGTCTG and TTCTGCTCAGTGTCCACGTC; *Aip*, ATGCGTGAGGGGGAGATT and TGGCCACTAGAGGATACAGGAC; *Cxxc1*, TCTGTGAGCGGAGATATGGA and TCCCCATTCTCAGACTTGCT; *Rn45s*, CGGACACGGACAGGATTGACA and ACCACCCACGGAATCGAGAAA; and *Rps20*, GGCATTTAAAGATACCGGAAAG and GTCCGCACAAACCTTCT. Except for the *Rest* primers, which do not amplify transcript uc029vis.1, all primer pairs amplify all UCSC isoforms of the gene (mm10).

Statistical Analysis. Statistical analyses were performed using Prism 5 (GraphPad). Western blots, MKI67+ width measurements in *Insm1*$^{+/+}$ and *Insm1*$^{-/-}$ embryos, MAP2+ proportions, and OLIG2+ cell counts were each analyzed using *t* tests. MKI67+ and MKI67− cell counts were analyzed using *t* tests with Welch's correction. Body weights, brain weights, and the MKI67+ width measurements in Nes-Cre, *Rcor1/2* fl, and *Rcor1/2* KO embryos were analyzed using one-way ANOVA followed by Tukey's multiple comparison tests. RT-qPCR data were $\log_2$-transformed before statistical analysis. Nes-Cre, *Rcor1/2* fl, *Rcor1/2* KO, and *Rest* rescue cDNA samples were compared with one-way ANOVA followed by Tukey's multiple comparison tests. *Insm1*$^{+/+}$ and *Insm1*$^{-/-}$ cDNA samples were compared using *t* tests with Welch's correction. Throughout the text, experimental results are expressed as mean ± SD.

ACKNOWLEDGMENTS. We are grateful for the support and helpful ongoing discussions of the work by Dr. John Rubenstein (University of California, San Francisco) and Dr. Huilan Yao (H3 Biomedicine). We thank Dr. Carmen Birchmeier at the Max Delbrück Center for Molecular Medicine for generously providing us with INSM1 antibody and Susan Kim for assisting with image analysis. This work was supported by NIH Grants NS022518 (to G.M.), UL1TR000128 (to S.K.M.), and NS093066 and DK09949 (to M.G.R.).

1. Andrés ME, et al. (1999) CoREST: A functional corepressor required for regulation of neural-specific gene expression. *Proc Natl Acad Sci USA* 96(17):9873–9878.
2. Qureshi IA, Gokhan S, Mehler MF (2010) REST and CoREST are transcriptional and epigenetic regulators of seminal neural fate decisions. *Cell Cycle* 9(22):4477–4486.
3. Su X, Kameoka S, Lentz S, Majumder S (2004) Activation of REST/NRSF target genes in neural stem cells is sufficient to cause neuronal differentiation. *Mol Cell Biol* 24(18): 8018–8025.
4. Otto SJ, et al. (2007) A new binding motif for the transcriptional repressor REST uncovers large gene networks devoted to neuronal functions. *J Neurosci* 27(25): 6729–6739.
5. Ballas N, Grunseich C, Lu DD, Speh JC, Mandel G (2005) REST and its corepressors mediate plasticity of neuronal gene chromatin throughout neurogenesis. *Cell* 121(4): 645–657.
6. Abrajano JJ, et al. (2010) Corepressor for element-1-silencing transcription factor preferentially mediates gene networks underlying neural stem cell fate decisions. *Proc Natl Acad Sci USA* 107(38):16685–16690.
7. Abrajano JJ, et al. (2009) REST and CoREST modulate neuronal subtype specification, maturation and maintenance. *PLoS One* 4(12):e7936.
8. Covey MV, Streb JW, Spektor R, Ballas N (2012) REST regulates the pool size of the different neural lineages by restricting the generation of neurons and oligodendrocytes from neural stem/progenitor cells. *Development* 139(16):2878–2890.
9. Abrajano JJ, et al. (2009) Differential deployment of REST and CoREST promotes glial subtype specification and oligodendrocyte lineage maturation. *PLoS One* 4(11):e7665.
10. You A, Tong JK, Grozinger CM, Schreiber SL (2001) CoREST is an integral component of the CoREST-human histone deacetylase complex. *Proc Natl Acad Sci USA* 98(4): 1454–1458.
11. Hakimi MA, et al. (2002) A core-BRAF35 complex containing histone deacetylase mediates repression of neuronal-specific genes. *Proc Natl Acad Sci USA* 99(11): 7420–7425.
12. Shi YJ, et al. (2005) Regulation of LSD1 histone demethylase activity by its associated factors. *Mol Cell* 19(6):857–864.
13. Consortium U (2015) UniProt: A hub for protein information. *Nucleic Acids Res* 43(Database issue):D204–D212.
14. Barrios AP, et al. (2014) Differential properties of transcriptional complexes formed by the CoREST family. *Mol Cell Biol* 34(14):2760–2770.
15. Zeng W, Kong Q, Li C, Mao B (2010) Xenopus RCOR2 (REST corepressor 2) interacts with ZMYND8, which is involved in neural differentiation. *Biochem Biophys Res Commun* 394(4):1024–1029.
16. Saleque S, Kim J, Rooke HM, Orkin SH (2007) Epigenetic regulation of hematopoietic differentiation by Gfi-1 and Gfi-1b is mediated by the cofactors CoREST and LSD1. *Mol Cell* 27(4):562–572.
17. Yang P, et al. (2011) RCOR2 is a subunit of the LSD1 complex that regulates ESC property and substitutes for SOX2 in reprogramming somatic cells to pluripotency. *Stem Cells* 29(5):791–801.
18. Nechiporuk T, et al. (2016) The REST remodeling complex protects genomic integrity during embryonic neurogenesis. *eLife* 5:e09584.
19. Tronche F, et al. (1999) Disruption of the glucocorticoid receptor gene in the nervous system results in reduced anxiety. *Nat Genet* 23(1):99–103.
20. Yao H, et al. (2014) Corepressor Rcor1 is essential for murine erythropoiesis. *Blood* 123(20):3175–3184.
21. Kessaris N, et al. (2006) Competing waves of oligodendrocytes in the forebrain and postnatal elimination of an embryonic lineage. *Nat Neurosci* 9(2):173–179.
22. Roy K, et al. (2004) The Tlx gene regulates the timing of neurogenesis in the cortex. *J Neurosci* 24(38):8333–8345.
23. Guy J, Hendrich B, Holmes M, Martin JE, Bird A (2001) A mouse Mecp2-null mutation causes neurological symptoms that mimic Rett syndrome. *Nat Genet* 27(3):322–326.
24. Welcker JE, et al. (2013) Insm1 controls development of pituitary endocrine cells and requires a SNAG domain for function and for recruitment of histone-modifying factors. *Development* 140(24):4947–4958.
25. Duggan A, et al. (2008) Transient expression of the conserved zinc finger gene INSM1 in progenitors and nascent neurons throughout embryonic and adult neurogenesis. *J Comp Neurol* 507(4):1497–1520.
26. Farkas LM, et al. (2008) Insulinoma-associated 1 has a panneurogenic role and promotes the generation and expansion of basal progenitors in the developing mouse neocortex. *Neuron* 60(1):40–55.
27. Osipovich AB, et al. (2014) Insm1 promotes endocrine cell differentiation by modulating the expression of a network of genes that includes Neurog3 and Ripply3. *Development* 141(15):2939–2949.
28. McGann JC, et al. (2014) Polycomb- and REST-associated histone deacetylases are independent pathways toward a mature neuronal phenotype. *eLife* 3:e04235.
29. Johnson R, et al. (2008) REST regulates distinct transcriptional networks in embryonic and neural stem cells. *PLoS Biol* 6(10):e256.
30. Grimes JA, et al. (2000) The co-repressor mSin3A is a functional component of the REST-CoREST repressor complex. *J Biol Chem* 275(13):9461–9467.
31. Tontsch S, Zach O, Bauer HC (2001) Identification and localization of M-CoREST (1A13), a mouse homologue of the human transcriptional co-repressor CoREST, in the developing mouse CNS. *Mech Dev* 108(1-2):165–169.
32. Wang Y, et al. (2016) LSD1 co-repressor Rcor2 orchestrates neurogenesis in the developing mouse brain. *Nat Commun* 7:10481.
33. Breslin MB, Zhu M, Notkins AL, Lan MS (2002) Neuroendocrine differentiation factor, IA-1, is a transcriptional repressor and contains a specific DNA-binding domain: identification of consensus IA-1 binding sequence. *Nucleic Acids Res* 30(4):1038–1045.
34. Zhang T, Liu WD, Saunee NA, Breslin MB, Lan MS (2009) Zinc finger transcription factor INSM1 interrupts cyclin D1 and CDK4 binding and induces cell cycle arrest. *J Biol Chem* 284(9):5574–5581.
35. Candal E, et al. (2007) Ol-insm1b, a SNAG family transcription factor involved in cell cycle arrest during medaka development. *Dev Biol* 309(1):1–17.
36. Gierl MS, Karoulias N, Wende H, Strehle M, Birchmeier C (2006) The zinc-finger factor Insm1 (IA-1) is essential for the development of pancreatic beta cells and intestinal endocrine cells. *Genes Dev* 20(17):2465–2478.
37. Wildner H, Gierl MS, Strehle M, Pla P, Birchmeier C (2008) Insm1 (IA-1) is a crucial component of the transcriptional network that controls differentiation of the sympatho-adrenal lineage. *Development* 135(3):473–481.
38. Ramachandran R, Zhao XF, Goldman D (2012) Insm1a-mediated gene repression is essential for the formation and differentiation of Müller glia-derived progenitors in the injured retina. *Nat Cell Biol* 14(10):1013–1023.
39. Forbes-Osborne MA, Wilson SG, Morris AC (2013) Insulinoma-associated 1a (Insm1a) is required for photoreceptor differentiation in the zebrafish retina. *Dev Biol* 380(2): 157–171.
40. Jia S, Wildner H, Birchmeier C (2015) Insm1 controls the differentiation of pulmonary neuroendocrine cells by repressing Hes1. *Dev Biol* 408(1):90–98.
41. Korutla L, Degnan R, Wang P, Mackler SA (2007) NAC1, a cocaine-regulated POZ/BTB protein interacts with CoREST. *J Neurochem* 101(3):611–618.
42. Saijo K, et al. (2009) A Nurr1/CoREST pathway in microglia and astrocytes protects dopaminergic neurons from inflammation-induced death. *Cell* 137(1):47–59.
43. Ying G, et al. (2009) The protocadherin gene Celsr3 is required for interneuron migration in the mouse forebrain. *Mol Cell Biol* 29(11):3045–3061.
44. Bai J, et al. (2003) RNAi reveals doublecortin is required for radial migration in rat neocortex. *Nat Neurosci* 6(12):1277–1283.
45. Kerjan G, et al. (2009) Mice lacking doublecortin and doublecortin-like kinase 2 display altered hippocampal neuronal maturation and spontaneous seizures. *Proc Natl Acad Sci USA* 106(16):6766–6771.
46. Huang Y, Myers SJ, Dingledine R (1999) Transcriptional repression by REST: Recruitment of Sin3A and histone deacetylase to neuronal genes. *Nat Neurosci* 2(10): 867–872.
47. Ballas N, et al. (2001) Regulation of neuronal traits by a novel transcriptional complex. *Neuron* 31(3):353–365.
48. Greenway DJ, Street M, Jeffries A, Buckley NJ (2007) RE1 Silencing transcription factor maintains a repressive chromatin environment in embryonic hippocampal neural stem cells. *Stem Cells* 25(2):354–363.
49. Mulligan P, et al. (2008) CDYL bridges REST and histone methyltransferases for gene repression and suppression of cellular transformation. *Mol Cell* 32(5):718–726.
50. Mandel G, et al. (2011) Repressor element 1 silencing transcription factor (REST) controls radial migration and temporal neuronal specification during neocortical development. *Proc Natl Acad Sci USA* 108(40):16789–16794.
51. Kuang C, et al. (2006) Intragenic deletion of Tgif causes defectsin brain development. *Hum Mol Genet* 15(24):3508–3519.
52. Sakamoto M, Hirata H, Ohtsuka T, Bessho Y, Kageyama R (2003) The basic helix-loop-helix genes Hesr1/Hey1 and Hesr2/Hey2 regulate maintenance of neural precursor cells in the brain. *J Biol Chem* 278(45):44808–44815.
53. Shen J, Walsh CA (2005) Targeted disruption of Tgif, the mouse ortholog of a human holoprosencephaly gene, does not result in holoprosencephaly in mice. *Mol Cell Biol* 25(9):3639–3647.
54. Wu J, Duggan A, Chalfie M (2001) Inhibition of touch cell fate by egl-44 and egl-46 in C. elegans. *Genes Dev* 15(6):789–802.
55. Jarriault S, Greenwald I (2002) Suppressors of the egg-laying defective phenotype of sel-12 presenilin mutants implicate the CoREST corepressor complex in LIN-12/Notch signaling in C. elegans. *Genes Dev* 16(20):2713–2728.
56. Desai C, Horvitz HR (1989) Caenorhabditis elegans mutants defective in the functioning of the motor neurons responsible for egg laying. *Genetics* 121(4):703–721.
57. Tuoc TC, et al. (2013) Chromatin regulation by BAF170 controls cerebral cortical size and thickness. *Dev Cell* 25(3):256–269.
58. Porteus MH, Bulfone A, Ciaranello RD, Rubenstein JL (1991) Isolation and characterization of a novel cDNA clone encoding a homeodomain that is developmentally regulated in the ventral forebrain. *Neuron* 7(2):221–229.
59. Sciavolino PJ, et al. (1997) Tissue-specific expression of murine Nkx3.1 in the male urogenital system. *Dev Dyn* 209(1):127–138.
60. Liao Y, Smyth GK, Shi W (2013) The Subread aligner: Fast, accurate and scalable read mapping by seed-and-vote. *Nucleic Acids Res* 41(10):e108.
61. Liao Y, Smyth GK, Shi W (2014) featureCounts: An efficient general purpose program for assigning sequence reads to genomic features. *Bioinformatics* 30(7):923–930.
62. Robinson MD, McCarthy DJ, Smyth GK (2010) edgeR: A Bioconductor package for differential expression analysis of digital gene expression data. *Bioinformatics* 26(1): 139–140.
63. Benjamini Y, Hochberg Y (1995) Controlling the false discovery rate: A practical and powerful approach to multiple testing. *J R Stat Soc Series B Stat Methodol* 57(1): 289–300.